Watt-level continuous-wave and passively *Q*-switched red lasers pumped by a single blue laser diode

Yuxia Zhang (张玉霞)[1], Yilun Yang (杨依伦)[2], Lianhan Zhang (张连翰)[2], Dazhi Lu (路大治)[1], Min Xu (徐 民)[2], Yin Hang (杭 寅)[2], Shishen Yan (颜世申)[3], Haohai Yu (于浩海)[1,*], and Huaijin Zhang (张怀金)[1,]**

[1]*State Key Laboratory of Crystal Materials and Institute of Crystal Materials, Shandong University, Jinan 250100, China*

[2]*Key Laboratory of High Power Laser Materials, Shanghai Institute of Optics and Fine Mechanics, Chinese Academy of Sciences, Shanghai 201800, China*

[3]*College of Physics and State Key Laboratory of Crystal Materials, Shandong University, Jinan 250100, China*

**Corresponding author: haohaiyu@sdu.edu.cn; **corresponding author: huaijinzhang@sdu.edu.cn*

Received January 27, 2019; accepted March 22, 2019; posted online May 8, 2019

Praseodymium-ion-doped gain materials have the superiority of lasing at various visible wavelengths directly. Simple and compact visible lasers are booming with the development of blue laser diodes in recent years. In this Letter, we demonstrate the watt-level red laser with a single blue laser diode and Pr:$YLiF_4$ crystal. On this basis, the passively *Q*-switched pulse lasers are obtained with monolayer graphene and Co:ZnO thin film as the *Q*-switchers in the visible range.

OCIS codes: 140.3480, 140.3540, 140.7300.
doi: 10.3788/COL201917.071402.

Visible lasers have many applications due to their unique properties of visibility. With this feature, visible lasers have broad applications in medical treatment, communication, our daily life, etc.[1–3]. Most rare-earth ions have the effective stimulated emission in the visible range. Among them, the Pr^{3+} ion is surely considered as a very attractive ion for the direct generation of visible laser because of the blue absorption and abundant visible emission transitions from 480 to 721 nm[4]. For Pr^{3+}-ion-doped crystals, the most common laser materials are fluoride crystals, of which $YLiF_4$ (YLF) crystal attracts the most studies and generates relatively high output power[5–7]. As characterizations of a continuous-wave (CW) laser, high power and high efficiency are main goals that the researchers pursue. Up to now, the watt-level CW outputs for Pr^{3+}-ion-doped crystals are generated with frequency-doubled optically pumped semiconductor lasers (2ω-OPSLs)[8], two blue laser diodes (LDs)[9], or four blue LDs[5–7] as the pump source, which probably give rise to the problem of cost. Up to now, there is still no watt-level output with a single blue LD as the pump source. Considering the cost control, we believe that the development of miniaturized high efficiency visible lasers with a simple pump source has perspective applications in many kinds of fields.

There are numerous conditions where the larger pulse energy and high peak power are required, and *Q*-switched pulse lasers emerged at the right moment. Along with the development of low-dimensional materials, atomic-layered transition-metal dichalcogenides *Q*-switchers[10,11], black phosphorus *Q*-switchers[12,13], quantum dots *Q*-switchers[14,15], topological insulator *Q*-switchers[16,17], etc. have been widely applied to generate visible pulse lasers with Pr^{3+}-ion-doped crystals or fibers according to previous reports in recent years. Graphene, as one of the earliest discovered two-dimensional materials, has been extensively utilized in *Q*-switching and mode-locking in the near-infrared range due to its excellent photoelectric properties accompanied by the peculiarity of zero bandgap[18,19]. Heretofore, with a graphene thin film as the *Q*-switcher, only a *Q*-switched orange laser at 603 nm using Pr^{3+}-ion-doped waterproof fluoride glass fiber was reported in 2014[20]. By using graphene oxide as the *Q*-switcher, the Pr^{3+}-ion-doped all-fiber *Q*-switched laser was obtained with the pulse energy of 24.2 nJ in the visible range[21]. There are still no reports about all-solid-state visible pulse lasers with graphene as the *Q*-switcher, which are worth studying. Meanwhile, a new research reported the passively *Q*-switched Pr:YLF lasers at multiple visible wavelengths with a Co^{2+}:$MgAl_2O_4$ crystal as the *Q*-switcher and 2ω-OPSL as the pump source[22]. This result proved the feasibility of Co^{2+} ion as the *Q*-switchers in the visible range. Hence, inspired by this, much more Co^{2+} ion *Q*-switchers can be investigated. Given the variety of nonlinear optical materials, a simple selection criterion for *Q*-switchers in the visible range would be useful concerning the relationship between the laser resonator, laser gain materials, and modulation materials.

In this Letter, a watt-level Pr:YLF visible laser was reported with a single blue LD, which was a miniaturized all-solid-state visible laser. The CW output power of the red and deep red lasers was obtained, respectively. A simple selection criterion for *Q*-switchers was introduced and a *Q*-switching standard for Pr^{3+}-ion-doped laser materials was calculated in the visible range, which may give

guidance for the research of Q-switchers in the visible range. On this basis, the passively Q-switched pulse lasers were obtained with monolayer graphene and Co:ZnO epitaxial thin film as the Q-switchers at 638 and 721 nm, respectively, for the first time, to the best of our knowledge.

The crystal used in this experiment was Pr:YLF grown with the Czochralski method. The concentration of Pr^{3+} ions in this work was 3% with the segregation coefficient of 0.1. The crystal was a cut with dimensions of 3 mm × 3 mm × 10 mm ($a \times c \times a$), corresponding to a relatively high absorptivity of 91%–97%. The 3 mm × 3 mm end surfaces were polished with high precision. The crystal was enclosed by indium foil and mounted in a copper block kept at 2°C before being inserted into the cavity. The pump source used in this experiment was a single blue LD with the maximum output power of 3.5 W. Unfortunately, the wavelength of the pump source increases with the increase of output power, leading to a decrease in the crystal absorption at 3.5 W. Therefore, the actual incident pump power is 3.1 W, corresponding to a wavelength of 443 nm in this experiment. The quality of the initial blue LD beam spot is poor, so a shaping system is necessary. The spot of the blue LD was collimated by a 4.51 mm focal length aspheric lens F1 (Thorlabs, C230TMD-A) and shaped into a circular beam by a pair of cylindrical lenses F2 and F3 with focal lengths of −20 mm (Thorlabs, LK1085L2-A) and 100 mm (Thorlabs, LJ1567RM-A), respectively. Then, the pump beam was focused into the crystal by a focusing lens F4 with a focal length of 50.8 mm. The focal spot radius in the crystal was about 48 μm × 50 μm with a better optical quality, which was beneficial for mode matching. The laser cavity was a simple plano-concave cavity, as shown in Fig. 1. The input mirror M1 is a plane mirror antireflection coated for the pump wavelength of 443 nm, and it is highly reflective for the laser wavelength (500–780 nm). The output coupler M2 is a plano-concave mirror coated for part transmission in accordance with requirements, and the curve radius is 50 mm. The cavity length is finally optimized to be about 42 mm in the following experiments. The laser output power was measured by a power meter (Newport, Model 1916-R). When measuring the output power, a filter was added in front of the power meter to eliminate pump light with a transmittance of 90% at 638 nm. Meanwhile, the laser spectrum was monitored by a spectrometer (Ocean Optics, HR4000).

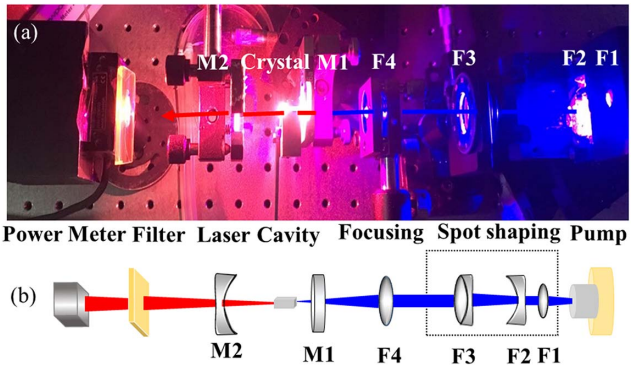

Fig. 1. CW experiment device of single blue LD pumped Pr:YLF laser. (a) Experimental configuration; (b) schematic diagram.

For the 638 nm red laser, the output coupler M2 was coated for part transmission with a transmittance of 1.8% at 638 nm. When the absorbed pump power increased to 214 mW, the red laser came out as shown in Fig. 2(a). By increasing the pump power and optimizing the laser cavity, a watt-level red laser was achieved (filter in mind). The maximum output power was about 1.05 W under the absorbed pump power of 2.89 W with a corresponding slope efficiency of 42.4%. The center wavelength is 638.1 nm, as shown in Fig. 2(b). To the best of our knowledge, this is the maximum output power of visible lasers with a single blue LD as the pump source. For the 721 nm deep red laser, the output coupler M2 was coated for part transmission with a transmittance of 2% at 721 nm. The threshold was measured to be 155 mW, and the maximum output power was 711 mW under the absorbed pump power of 2.89 W, as shown in Fig. 2(c). The slope efficiency was about 28.6%, and the center wavelength is 721.1 nm, as shown in Fig. 2(d).

Based on the analysis of our previous Letter, the selection criterion of Q-switchers can be written as in Refs. [23–26]:

$$F_{\mathrm{sat},A}/\Delta R\tau_A \le \frac{2hc\omega_{\mathrm{eff},L}^2}{m\lambda\sigma_{\mathrm{em},L}\omega_{\mathrm{eff},A}^2 T_R}, \tag{1}$$

where $F_{\mathrm{sat},A}$ is the saturation fluence of the Q-switcher, τ_A is the recovery time of the Q-switcher, T_R is laser cavity round-trip time, ΔR is the modulation depth, which is the transmission or reflection difference between the saturated and initial states of the Q-switcher, $\sigma_{\mathrm{em},L}$ is the emission cross section of the laser gain material, $\omega_{\mathrm{eff},L}$ and $\omega_{\mathrm{eff},A}$ are the effective radii on the laser gain material and

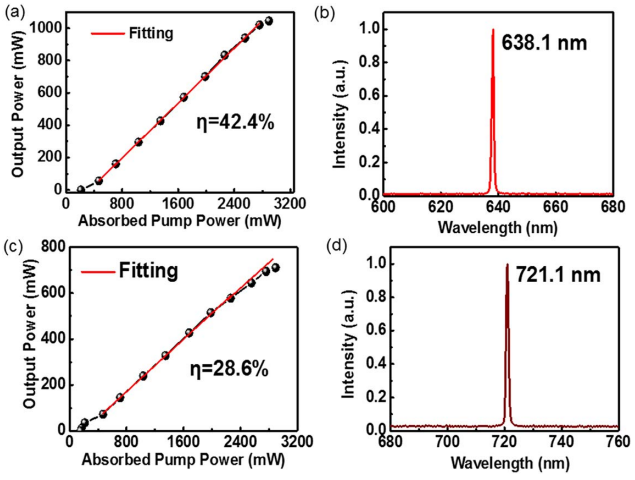

Fig. 2. Results of CW lasers. (a) Output power versus absorbed pump power for 638.1 nm red laser; (b) spectrum of the red output laser; (c) output power versus absorbed pump power for 721.1 nm deep red laser; (d) spectrum of the deep red output laser.

Q-switcher, respectively, $m = 1$ for the ring cavity, $m = 2$ for the linear cavity, h is the Planck constant, c is the speed of light in vacuum, and λ is the wavelength of laser. In Eq. (1), the left-hand side is the intrinsic characteristics of the Q-switcher, which can be measured with appropriate experimental methods. The right-hand side is the optical parameters about the laser gain material and laser cavity. The overwhelming superiority of this equation is the independence of the laser cavity design and Q-switcher choosing in a Q-switched pulse laser.

In this Q-switching experiment, if the laser gain material is a Pr^{3+}-ion-doped crystal, the emission cross section is in a magnitude of 10^{-20} cm^2. The Q-switcher is inserted close to the output coupler, and the laser cavity is a linear two-mirror cavity with the optimized length of 42 mm; thus, the Gaussian beam radius can be estimated to be 60 and 140 μm on Pr:YLF and Q-switcher, respectively. Then, the right-hand side of Eq. (1) can be calculated to be 1.78 and 1.57 mJ/(cm^2 · ps) for 638 and 721 nm. That is to say, based on the cavity and crystal we have proposed, the Q-switcher must satisfy the following conditions:

$$F_{\mathrm{sat},A}/\Delta R\tau_A \le 1.57\ \mathrm{mJ/(cm^2 \cdot ps)}. \tag{2}$$

In this experiment, monolayer graphene and Co:ZnO epitaxial thin film were selected as the Q-switchers in the visible range. The monolayer graphene used here was prepared by chemical vapor deposition method and transferred to a sapphire substrate with dimensions of 10 mm × 10 mm × 0.3 mm (SixCarbon Technology). The fabricated monolayer graphene was shown in the inset of Fig. 3(a). For investigating the optical response of the prepared monolayer graphene/sapphire sample in the visible range, the transmission spectrum was measured with a spectrophotometer (Hitachi, U-3500) from 400 to 800 nm, as shown in Fig. 3(a). The transmission spectrum of the empty sapphire substrate was also measured for comparison. The transmission of monolayer graphene was stable with the value of 77% in the visible range. Meanwhile, the doping concentration of Co^{2+} was 16% for Co:ZnO epitaxial thin film. The sample was fabricated by the molecular beam epitaxy method with Al_2O_3 (0001) as the substrate, and the dimensions were 10 mm × 5 mm × 0.5 mm, as shown in the inset of Fig. 3(b). The sample appears light green in natural light with uniform thickness and a smooth surface. Applying the same measurement, the transmission spectra of Co:ZnO and ZnO were obtained, as shown in Fig. 3(b). As can be seen in this figure, the 16% Co:ZnO has strong absorption at the wavelength of 660 nm compared with pure ZnO. The absorption can be ascribed to the spin and electric-dipole-allowed $^4A_2(^4F) \rightarrow {}^4T_1(^4P)$ in the visible range[27]. The transmission at 660 nm is about 61%, which was a little low when in the case of the intracavity. For 721 nm, the transmission is about 75%.

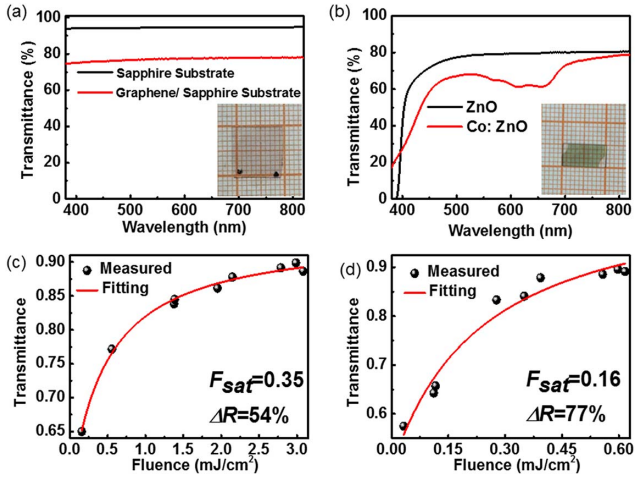

Fig. 3. Optical characterizations of prepared monolayer graphene and Co:ZnO epitaxial thin film. (a) Transmission spectra of monolayer graphene/sapphire and sapphire substrate (inset: picture of prepared monolayer graphene sample); (b) transmission spectra of 16% Co:ZnO and pure ZnO (inset: picture of prepared Co:ZnO sample); (c) trend of transmittance with the incident fluence for monolayer graphene at 532 nm; (d) trend of transmittance with the incident fluence for Co:ZnO at 532 nm.

For the research of the nonlinear optical properties of monolayer graphene and Co:ZnO epitaxial thin film, the saturable absorption measurements were performed with a nanosecond laser (Opolette HE 355 II). The excitation source has a pulse width of 10 ns and a repetition rate of 20 Hz. The beam was focused on the sample with a focusing lens, and the radius was about 200 μm. The transmittance was obtained by measuring the energy before and after the sample and then calculating the ratio of the two values. By increasing the incident power, the transmittance tended to be saturated, as shown in Figs. 3(c) and 3(d), for monolayer graphene and Co:ZnO epitaxial thin film, respectively. The wavelength of incident light was tuned to 532 nm. Associated with the relationship between the photo-induced electron-hole density and the irradiation light intensity, the absorption coefficient can be shown as in Ref. [28]:

$$\alpha = \frac{\alpha_S}{1 + \frac{F}{F_{\mathrm{sat},A}}} + \alpha_{\mathrm{NS}}, \tag{3}$$

where α_S and α_{NS} are the saturable and unsaturable absorption coefficients, respectively. F is the irradiation fluence, and $F_{\mathrm{sat},A}$ is the saturable irradiation fluence. Therefore, the fluence-dependent transmission can be shown in the form as

$$T(F) = \exp(-\alpha d) = A \exp\left(-\frac{\Delta T}{1 + \frac{F}{F_{\mathrm{sat},A}}}\right), \tag{4}$$

where d is the thickness of the sample, $A = \exp(-\alpha_{\mathrm{NS}} d)$ is the unsaturable absorption, and $\Delta T = \alpha_S d$ is the normalized modulation depth. The modulation depth ΔR, which indicates the difference between the final and initial transmission can be expressed as

$$\Delta R = T(F \to \infty) - T(F \to 0)\, A\Delta T. \tag{5}$$

Fitting by Eq. (4), the saturable irradiation fluence $F_{\mathrm{sat},A}$, modulation depth ΔT, and unsaturable absorption A were calculated to be 0.35 mJ/cm^2, 54%, 0.94 and 0.16 mJ/cm^2, 77%, 0.99 for monolayer graphene and Co:ZnO epitaxial thin film, respectively. The recovery time of monolayer graphene and Co:ZnO was 1 and 0.9 ps based on the previous report[29,30]. Then, the left-hand side of Eq. (1) can be calculated as 0.69 mJ/(cm^2 · ps) and 0.23 mJ/(cm^2 · ps) for monolayer graphene at 638 nm and Co:ZnO epitaxial thin film at 721 nm, respectively, which meet the requirements of Eq. (2). This implies that the prepared samples are suitable Q-switchers for Pr:YLF Q-switching in the visible range.

For the monolayer graphene Q-switcher, by inserting the sample into the cavity close to the output coupler M2 and increasing the pump power continuously, the red pulse laser at 638 nm was obtained with the threshold of 246 mW. The increasing trend of average output power with the absorbed pump power was shown in Fig. 4(a). As can be seen in the figure, the maximum average output power was 17 mW under the absorbed pump power of 872 mW. If the pump power continues to increase, the pulses will become unstable as observed by the oscilloscope. With increasing the absorbed pump power, variations of repetition rate and pulse width were recorded with the help of a digital oscilloscope (Tektronix, MSO 72504DX) and silicon detector, as shown in Fig. 4(b). In the figure, the repetition rate increased while the pulse width decreased along with the absorbed pump power augmentation, which is typical in passive Q-switching. The calculated repetition rate located in the range of 39–225 kHz and the typical pulse train recorded by the oscilloscope are shown in Fig. 4(c). The shortest pulse width was 709 ns under the absorbed pump power of 872 mW, as shown in Fig. 4(d). With the average output power and repetition rate, the pulse energy can be calculated with the maximum value of 0.2 μJ under an absorbed pump power of 790 mW.

In the same way as monolayer graphene, the deep red pulse laser at 721 nm was obtained with Co:ZnO epitaxial thin film as the Q-switcher. When the absorbed pump power was increased to 1.1 W, the deep red pulse laser appeared. The threshold of Co:ZnO epitaxial thin film was much higher compared with that of monolayer graphene at 638 nm. As can be seen in Fig. 5(a), the average output power had an increasing trend with the absorbed pump power, and the maximum average output power was 26 mW under the absorbed pump power of 2.2 W. If the pump power continues to increase, the pulse will also become unstable, as monitored by the oscilloscope. Just like the red pulse laser, the repetition rate of the deep red laser also behaved with an increasing trend with the increasing of the absorbed pump power, while the pulse width had the opposite tendency, as shown in Fig. 5(b). The repetition rate was in the range of 60–250 kHz, and the typical pulse train was shown in Fig. 5(c). The shortest pulse width was 586 ns under the absorbed pump power of 2.1 W, as shown in Fig. 5(d). With the average output power and repetition rate, the pulse energy could be calculated with the maximum value of 0.1 μJ under an absorbed pump power of 1.8 W. Compared with the monolayer graphene Q-switcher, the Co:ZnO epitaxial thin film Q-switcher has a much larger modulation depth, which is beneficial for modulation in the wide range. However, the transmission of Co:ZnO epitaxial thin film in the visible range is a little lower, which may result in large intracavity losses, eliminating effective output.

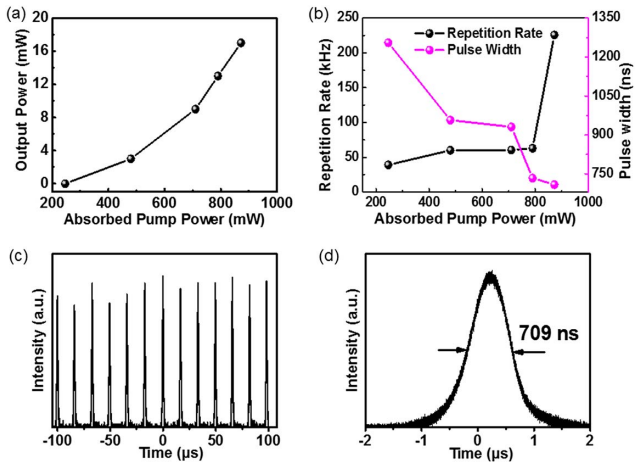

Fig. 4. Characterizations of the Q-switched pulse lasers with monolayer graphene as the Q-switcher at 638 nm. (a) Average output power versus absorbed pump power; (b) repetition rate and pulse width of the pulse laser versus absorbed pump power; (c) pulse train recorded by the oscilloscope; (d) single red pulse with the pulse width of 709 ns.

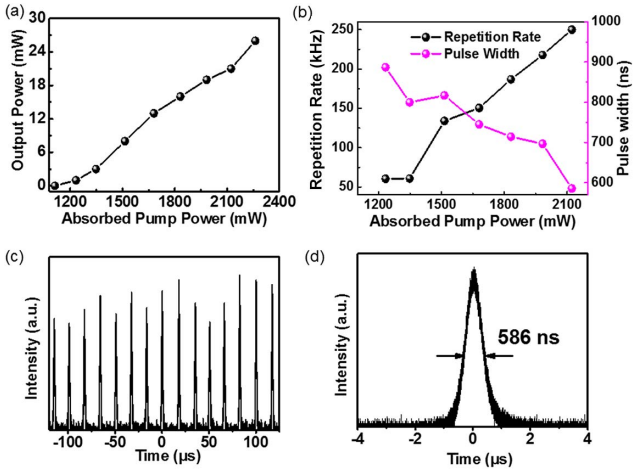

Fig. 5. Characterizations of the Q-switched pulse lasers with Co:ZnO as the Q-switcher at 721 nm. (a) Average output power versus absorbed pump power; (b) repetition rate and pulse width of the pulse laser versus absorbed pump power; (c) pulse train recorded by the oscilloscope; (d) single deep red pulse with the pulse width of 586 ns.

In conclusion, we have reported a watt-level visible laser output employing a Pr^{3+}-doped YLF crystal and a single blue LD, which is conducive to miniaturization and simplification of visible lasers. In terms of cost control, a single LD is much cheaper than multiple coupler LDs, and therefore, the research of directly generating a high power visible laser with a single LD pump source is still well worth investigating. The CW output powers of red and deep red lasers are 1.05 and 711 mW at 638 and 721 nm with the slope efficiencies of 42.4% and 28.6%, respectively. Based on the results of CW visible lasers, the passively *Q*-switched pulse lasers were obtained with monolayer graphene and Co:ZnO epitaxial thin film as the *Q*-switchers at 638 and 721 nm, respectively. In the passively *Q*-switched lasers, the maximum repetition rate and the minimum pulse width were 225 kHz, 709 ns and 250 kHz, 586 ns, with the maximum pulse energy of 0.1–0.2 μJ for 638 and 721 nm, respectively. Compared with mature *Q*-switchers of semiconductor saturable absorber mirror (SESAM) and $Cr:Y_3Al_5O_{12}$ (Cr:YAG), these experimental results are not very perfect[31,32]. Based on the advantages of easy preparation, low cost, etc., we believe that much better performance will be generated by optimizing the material design. In addition, we provide a simple selection criterion for the *Q*-switcher and calculate a standard for visible *Q*-switching, which can give guidance for the research of a *Q*-switcher in the visible range.

This work was supported by the National Key Research and Development Program of China (Nos. 2016YFB0701002 and 2016YFB1102301) and the National Natural Science Foundation of China (NSFC) (Nos. 51772173, 51632004, 51472257, and 51872307).

References

1. K. V. Chellappan, E. Erden, and H. Urey, Appl. Opt. **49**, F79 (2010).
2. D. Anguita, D. Brizzolara, and G. Parodi, in *Oceans* (2010), p. 1.
3. R. G. Wheeland, Laser. Surg. Med. **16**, 2 (1995).
4. M. J. Weber, *Handbook of Lasers* (CRC Press, 2000).
5. S. Luo, X. Yan, Q. Cui, B. Xu, H. Xu, and Z. Cai, Opt. Commun. **380**, 357 (2016).
6. H. Tanaka, S. Fujita, and F. Kannari, Appl. Opt. **57**, 5923 (2018).
7. K. Iijima, R. Kariyama, H. Tanaka, K. Hirosawa, and F. Kannari, in *Conference on Lasers and Electro-Optics/Pacific Rim* (Optical Society of America, 2015), paper 25B3_5.
8. P. W. Metz, F. Reichert, F. Moglia, S. Muller, D. T. Marzahl, C. Krankel, and G. Huber, Opt. Lett. **39**, 3193 (2014).
9. S. Luo, B. Xu, H. Xu, and Z. Cai, Appl. Opt. **56**, 9552 (2017).
10. B. Guo, Chin. Opt. Lett. **16**, 020004 (2018).
11. W. Li, J. Peng, Y. Zhong, D. Wu, H. Lin, Y. Cheng, Z. Luo, J. Weng, H. Xu, and Z. Cai, Opt. Mater. Express **6**, 2031 (2016).
12. R. Zhang, Y. Zhang, H. Yu, H. Zhang, R. Yang, B. Yang, Z. Liu, and J. Wang, Adv. Opt. Mater. **3**, 1787 (2015).
13. D. Wu, Z. Cai, Y. Zhong, J. Peng, Y. Cheng, J. Weng, Z. Luo, and H. Xu, IEEE J. Sel. Top. Quant. **23**, 0900106 (2017).
14. J. Li, H. Dong, B. Xu, S. Zhang, Z. Cai, J. Wang, and L. Zhang, Photon. Res. **5**, 457 (2017).
15. B. Xu, S. Luo, X. Yan, J. Li, J. Lan, Z. Luo, H. Xu, Z. Cai, H. Dong, and J. Wang, IEEE J. Sel. Top. Quant. **23**, 1900507 (2017).
16. Y. Cheng, J. Peng, X. Bin, H. Xu, Z. Cai, and J. Weng, Opt. Laser Technol. **88**, 275 (2017).
17. S. Luo, X. Yan, B. Xu, L. Xiao, H. Xu, Z. Cai, and J. Weng, Opt. Commun. **406**, 61 (2018).
18. Q. Bao, H. Zhang, Z. Ni, Y. Wang, L. Polavarapu, Z. Shen, Q. H. Xu, D. Tang, and K. P. Loh, Nano Res. **4**, 297 (2010).
19. Y. Wang, W. Chen, M. Mero, L. Zhang, H. Lin, Z. Lin, G. Zhang, F. Rotermund, Y. J. Cho, and P. Loiko, Opt. Lett. **42**, 3076 (2017).
20. Y. Fujimoto, T. Suzuki, R. Ochante, T. Hirayama, M. Murakami, H. Shiraga, M. Yoshida, O. Ishii, and M. Yamazaki, Electron. Lett. **50**, 1470 (2014).
21. Y. Zhong, Z. Cai, D. Wu, Y. Cheng, J. Peng, J. Weng, Z. Luo, B. Xu, and H. Xu, IEEE Photo. Tech. Lett. **28**, 1755 (2016).
22. M. Demesh, D. T. Marzahl, A. Yasukevich, V. Kisel, G. Huber, N. Kuleshov, and C. Krankel, Opt. Lett. **42**, 4687 (2017).
23. C. Hönninger, R. Paschotta, F. Morier-Genoud, M. Moser, and U. Keller, J. Opt. Soc. Am. B **16**, 46 (1999).
24. H. Haus, IEEE J. Quant. Electron. **12**, 169 (1976).
25. F. X. Kaertner, L. R. Brovelli, D. Kopf, M. Kamp, I. G. Calasso, and U. Keller, Opt. Eng. **34**, 2024 (1995).
26. Y. Zhang, D. Lu, H. Yu, and H. Zhang, Adv. Opt. Mater. **7**, 1800886 (2019).
27. N. Kuleshov, V. Mikhailov, V. Scherbitsky, P. Prokoshin, and K. Yumashev, J. Lumin. **55**, 265 (1993).
28. E. Garmire, IEEE J. Sel. Top. Quant. **6**, 1094 (2000).
29. P. Loiko, O. Dymshits, V. Vitkin, N. Skoptsov, A. Zhilin, D. Shemchuk, M. Y. Tsenter, K. Bogdanov, A. Malyarevich, and I. Glazunov, Appl. Opt. **55**, 5505 (2016).
30. J. M. Dawlaty, S. Shivaraman, M. Chandrashekhar, F. Rana, and M. G. Spencer, Appl. Phys. Lett. **92**, 042116 (2008).
31. H. Tanaka, R. Kariyama, K. Iijima, and F. Kannari, Appl. Opt. **55**, 6193 (2016).
32. V. G. Savitski, I. M. Ranieri, A. B. Krysa, and S. Calvez, in *CLEO: Science and Innovations* (Optical Society of America, 2011), paper CMB7.